Tribol Lett (2012) 46:65–73
DOI 10.1007/s11249-012-9918-7

ORIGINAL PAPER

Adhesion and Friction Studies of Nano-textured Surfaces Produced by Self-Assembling Au Nanoparticles on Silicon Wafers

Xiaoliang Zhang · Xiaohua Zhong · Xu Meng · Gewen Yi · Junhong Jia

Received: 8 April 2011 / Accepted: 16 January 2012 / Published online: 2 February 2012

Abstract This article presents the results of nanoscale friction and adhesion of nanoparticle-textured surfaces (NPTS) using atomic force microscope (AFM). The effects of coverage ratio, texture height, and packing density on the adhesion and friction of the NPTS were investigated. The nano-textured surfaces were produced by self-assembling Au nanoparticles (NPs) with diameters of 20 nm and 50 nm on the silicon (100) surfaces, respectively. Surface morphology of the NPTS was characterized by field emission scanning electron microscopy and AFM. The results show that the NPTS significantly reduced the adhesive force compared to the smooth surface. The adhesion of NPTS is mainly dependent on the coverage ratio of NPs rather than the texture height and higher coverage ratio resulted in smaller adhesive force. The reduced adhesion of textured surfaces was attributed to the reduced real area of contact. The friction of NPTS is mainly dependent on the spacing between asperities. The lowered frictional force was obtained when the spacing between asperities is less than the size of AFM tip, because of the effectively reduced real area of contact between the AFM tip and the NPTS surface.

X. Zhang · X. Zhong · X. Meng · G. Yi · J. Jia (✉)
State Key Laboratory of Solid Lubrication, Lanzhou Institute of Chemical Physics, Chinese Academy of Sciences, Lanzhou 730000, China
e-mail: jhjia@licp.cas.cn

X. Zhang
Graduate University of Chinese Academy of Sciences, Beijing 100049, China

X. Zhong · X. Meng
Lanzhou University of Technology, Lanzhou 730050, China

Keywords Surface modification · Adhesion · Nanotribology · AFM

1 Introduction

Many studies have shown that surface roughness affects the adhesive and frictional forces [1–3]. One effective approach of reducing adhesive and frictional forces between contacting interfaces is to create textured surfaces or surface modification, which is especially beneficial to micro/nano systems (e.g., MEMS/NEMS) that normally have smooth surfaces and are subjected to small applied forces [4–6]. In miniaturized systems, the adhesion contribution to friction can no longer be neglected because of the large surface area-to-volume ratio of structures and the increased surface smoothness. Actually, the adhesive force and frictional force are two of the main issues affecting the reliability of miniaturized devices involving contact interfaces. Therefore, a fundamental understanding of adhesive and frictional behaviors and controlling the adhesion and friction at nanoscale level are of great scientific and technological significance [7].

Surface texturing is an effective method to reduce adhesive force and frictional force in nanoscale which is attributed to the reduction of real area of contact between the contact and friction specimens. Various techniques have been used to fabricate the textured surfaces, including spin-coating [8], reactive ion etching [9], gas-expanded liquid [10], laser etching [11–16], template printing [7, 17, 18], self-assembly [19–23], and focused ion beam milling [24–26]. Zou et al. [8] prepared silicon oxide nano-textured surfaces using spin-coating technique and found that nano-textured surfaces have significantly smaller adhesion and friction because of the much reduced contact area. The

results also showed that tip size has a significant effect on the frictional behavior of the nano-textured surfaces. The coefficient of friction (COF) reduction measured by a larger tip is much larger than that measured by a smaller tip. Burton and Bhushan [3] prepared nano-patterned polymers using the template printing. They found that when the size of tip is larger than the spacing between asperities, the patterning can effectively reduce the real area of contact between the tip and sample surfaces and lead to reduced adhesion and friction. Singh and Yoon [17] prepared the polymethyl methacrylate (PMMA) micro-patterned surfaces using the leaf of lotus and taro and found that the patterned surfaces exhibited excellent wear resistance in microscale.

Self-assembly is one of the most simple, convenient, and reliable method to fabricate nano-textured surfaces [19–23, 27–31]. By altering the nanoparticles (NPs), coupling agents and substrates, they have prepared various patterned surfaces for applications in Raman scattering [19, 28–30], fluorescence emission [28], redox-active [27], and other fields [10, 32]. However, the nanoparticle-textures on the adhesive and frictional behaviors have not been systematically analyzed and investigated so far. Moreover, self-assembly has a unique advantage for controlling the adhesion and friction at nanoscale level by adjusting the nano-texture material, size, coverage ratio (packing density), and spacing between asperities. In the present study, Au NPs with diameters of 20–50 nm were assembled on the silicon (100) surfaces to explore the effects of the NPs' coverage ratio, packing density, textured height, and normal load on adhesive and frictional behaviors of nanoparticle-textured surfaces (NPTS). This study provides unique opportunities for fundamental nanoscale research on the adhesive and frictional phenomena of NPTS and guidance for further fundamental research study on nanotribology.

2 Experimental Details

2.1 Materials and Surface Processing

N-type single-crystal silicon (100) wafers with one side polished were purchased from Beijing GRINM semiconductor company. 3-Aminopropyl trimethoxysilane (APS, $\omega = 97\%$, $C_6H_{17}NO_3Si$) was purchased from Alfa Aesar company. All the other reagents were of analytic grade and used as received. Deionized water with the resistivity >18 MΩ cm was used throughout the experiment. Tetrachloroauric acid (5.44×10^{-3} M, $AuHCl_4$) and trisodium citrate solutions (5.00×10^{-3} M, $C_6H_5Na_3O_7$) were prepared first. Aqueous solution of Au NPs was prepared by citrate reduction of $HAuCl_4$ following the method of Frens [33], and the 20–50 nm Au NPs were prepared by using the different volume of citrate.

Before film deposition, the silicon substrates (1×1 cm^2) were ultrasonically cleaned by soaking in piranha-solution followed by thorough rinsing with deionized water, and drying with dry nitrogen. The cleaned substrates were immersed in methanol solution of 8.3 mM of APS for 24 h at room temperature, then rinsed with methanol and deionized water to remove any residual APS molecules, and dried with nitrogen. The silanized silicon wafers were dipped in a tube containing the freshly prepared Au colloidal suspension for a given time at room temperature to adhere the NPs onto the APS–SAMs surfaces. The substrates were then rinsed in deionized water and ultrasonically washed to remove the leftover Au precipitates, and dried with nitrogen gas. Finally, the APS–SAMs samples and all the NPTS samples were sputter-coated with a thin Au layer by JFC-1600 auto fine coater to eliminate the possible influence of the different surface chemical properties of APS film and Au nanoparticle on the adhesion and friction.

2.2 Characterization

Surface topography characterizations of the NPTS were performed by a field emission scanning electron microscopy (FESEM, JSM-6701F, Japan) and atomic force microscopy (AFM, Veeco Nanoscope IIIa Multimode, USA). Adhesive force (pull-off force) and frictional force investigations were conducted in air at room temperature with a relative humidity of about 30% using AFM. The tips used in adhesion and friction studies are Si_3N_4 tips with the spring constant of 0.3 N/m and the nominal radii of curvature of 20 nm. The deflection sensitivity of AFM tips is 43.69 nm/V. The average adhesion of at least 50 measurements for each sample is reported in this article. Friction tests were performed at the scanning frequency of 1 Hz (2 μm/s), loads of 7–60 nN, and scanning length of 1 μm. Each test was repeated at least 20 times, and the average of the output voltage signal represents the frictional force indirectly, which was acquired from the friction loop. The COF was defined as the ratio of the measured frictional force to the normal load.

3 Results and Discussion

3.1 Characterization of the Au Nanoparticle-Textured Surfaces

Figure 1 shows the AFM images (1×1 μm^2) of Au NPTS at different assembling time. It can be seen that the substrate surface is very homogeneous and smooth (Fig. 1a).

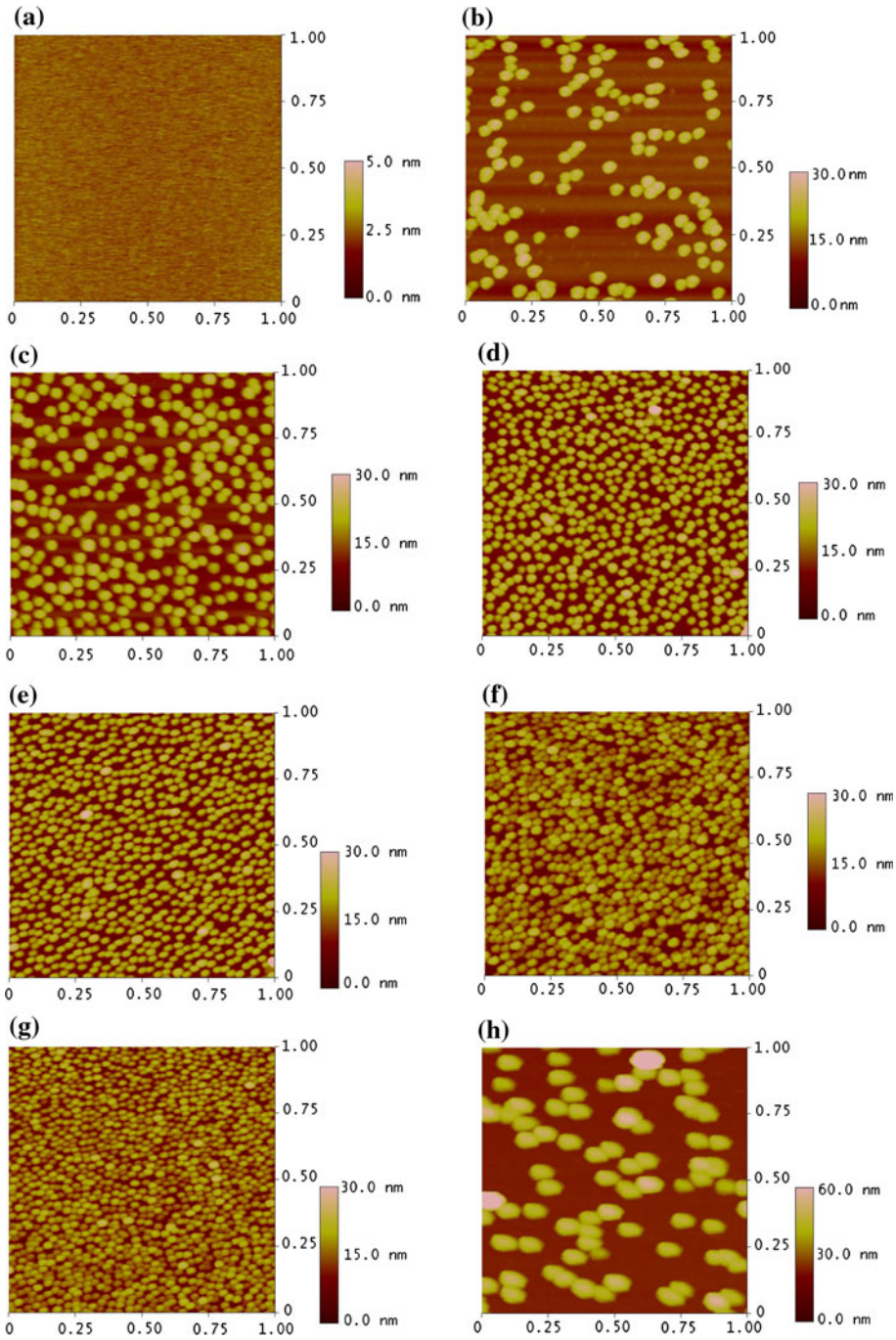

Fig. 1 AFM images (1×1 μm^2) of substrate surface and NPTS at different assembling times. **a** substrate surface, **b** 20 nm—0.5 h, **c** 20 nm—1.5 h, **d** 20 nm—3.0 h, **e** 20 nm—6.0 h, **f** 20 nm—12.0 h, **g** 20 nm—24.0 h, and **h** 50 nm—6.0 h

For the NPTS, the Au NPs are of spherical shape and randomly distributed on the silicon surfaces (Fig. 1b–g). The NPs coverage ratio γ (i.e., the ratio of area of NPs assembled on the substrate surface to area of substrate surface, %) increased with assembling time. The diameters of Au NPs are in the range of 32 ± 8 nm, which are considerably larger than those determined from TEM (not shown) and SEM (Fig. 2a) measurements of approximately 20 ± 3 nm. However, the section analysis performed on the AFM image demonstrates that their heights are approximately 20 nm, which is in agreement with the size of the NPs obtained from TEM or SEM analysis. It has been reported in the literature that such deviation is attributed to the "convolution effect" of true particles with the AFM tip, which is often observed in AFM imaging [30, 34]. Similarly, the 50 nm Au NPs are of spherical shape and randomly distributed on the silicon surface (Fig. 1h). The diameters of Au NPs are in the range of

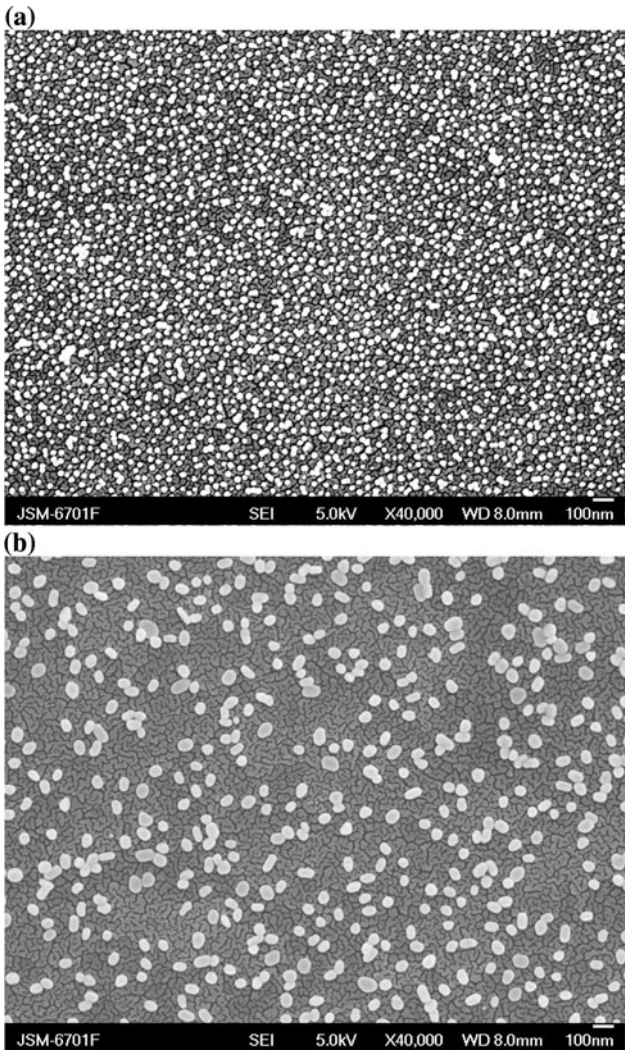

Fig. 2 FESEM images (×40,000) of 20 nm (**a**) and 50 nm (**b**) Au NPTS both at assembling time of 6.0 h

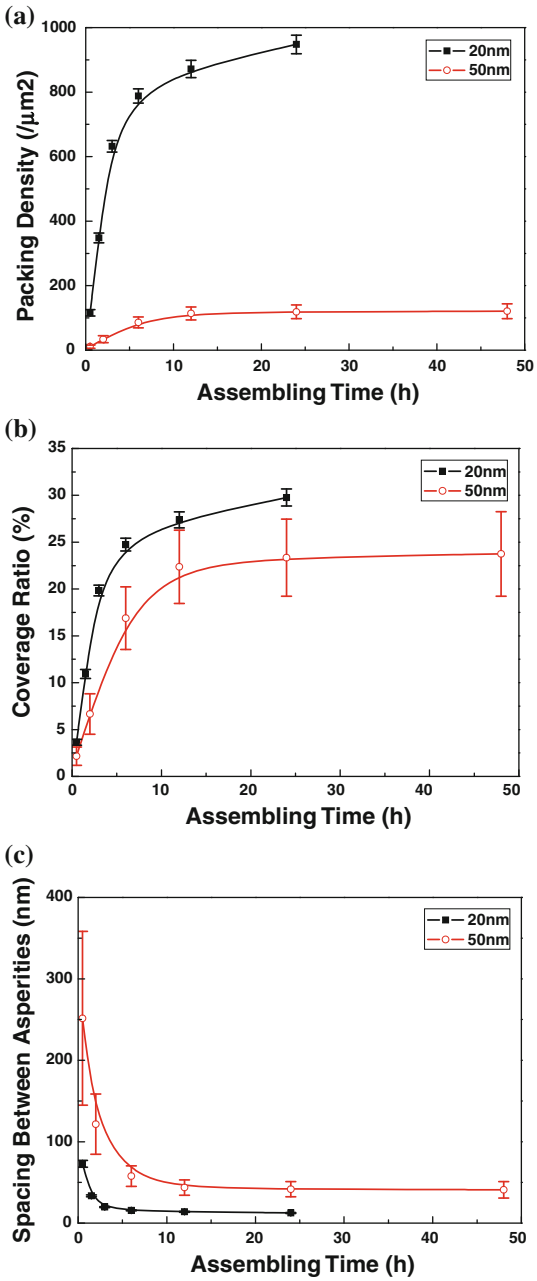

Fig. 3 The variation of packing density (**a**), coverage ratio (**b**), and spacing between asperities (**c**) for 20–50 nm Au NPTS at different assembling times

85 ± 10 nm in AFM image due to the "convolution effect" of AFM tip. It is also shown that the packing density ρ (i.e., the number of NPs assembled on the substrate surface in area of 1 × 1 $\mu m^2/\mu m^2$) of 50 nm NPs is still quite low even after the assembling time reaches to 6.0 h.

Figure 2 shows the FESEM images (×40,000) of 20 nm (Fig. 2a) and 50 nm (Fig. 2b) Au NPTS both at assembling time of 6.0 h, respectively. It can be seen that both of 20–50 nm Au NPs are of spherical shape and randomly distributed on the substrate surface. With the same assembling time of 6.0 h, the packing density of 20 nm NPs is much higher than that of 50 nm NPs, due to the larger weight and larger volume of 50 nm NPs.

Figure 3 shows the variations in geometrical parameters of 20–50 nm Au NPTS at different assembling times, including the packing density, the coverage ratio, and spacing between asperities. Tables 1, 2 show the detailed data of geometrical parameters of 20–50 nm Au NPTS determined by AFM images. The average surface coverage ratio γ (%) and average spacing between asperities δ (nm) were calculated from the following equations:

$$\gamma\ (\%\ ) = nS_{\mathrm{Au}}/S_{\mathrm{Si}} = n\pi R^2/S_{\mathrm{Si}} \quad (1)$$

$$\delta\ =\ (S_{\mathrm{Si}}/n)^{0.5} - 2R \quad (2)$$

where n is the number of Au NPs, R is the radius of Au nanoparticle, and S_{Si} is the area of Si (100). It is seen that

Table 1 Geometrical parameters of 20 nm Au NPTS

Assembling time t (h)	Packing density ρ (/μm^2)	Coverage ratio γ (%)	Spacing between asperities δ (nm)
0.5	116 ± 10	3.64 ± 0.31	72.85 ± 4.28
1.5	348 ± 15	10.93 ± 0.47	33.61 ± 1.19
3.0	632 ± 18	19.84 ± 0.57	19.78 ± 0.58
6.0	788 ± 22	24.74 ± 0.69	15.62 ± 0.51
12.0	872 ± 27	27.38 ± 0.85	13.86 ± 0.54
24.0	948 ± 29	29.77 ± 0.91	12.48 ± 0.51

Table 2 Geometrical parameters of 50 nm Au NPTS

Assembling time t (h)	Packing density ρ (/μm^2)	Coverage ratio γ (%)	Spacing between asperities δ (nm)
0.5	11 ± 5	2.16 ± 0.98	251.51 ± 106.74
2.0	34 ± 11	6.67 ± 2.16	121.50 ± 37.01
6.0	86 ± 17	16.88 ± 3.34	57.83 ± 12.56
12.0	114 ± 20	22.37 ± 3.92	43.66 ± 9.48
24.0	119 ± 21	23.35 ± 4.12	41.67 ± 9.35
48.0	121 ± 23	23.75 ± 4.51	40.91 ± 10.11

the packing density of NPs was increasing quickly during the assembling time of 0–6.0 h, after which it increased slightly with assembling time (Fig. 3a). There was a great difference in packing density between 20 and 50 nm NPTS at the same assembling time. The packing density of NPs for 20 nm Au NPTS assembled for 0.5 h is 116 ± 10/μm^2 which is approximately the same as that for 50 nm Au NPTS assembled for 12.0 h. Owing to the larger radii of curvature of 50 nm Au NPs, the difference in coverage ratio between 20 and 50 nm NPTS at the same assembling time is less than that in packing density as shown in Fig. 3b. For example, the coverage ratio for 20 nm Au NPTS assembled for 24.0 h is 29.77 ± 0.91%, while the coverage ratio for 50 nm Au NPTS assembled for 24.0 h is 23.35 ± 4.12%. Here, the surface coverage ratio of the NPs on the substrate could not reach 100%, which might be limited by inter-particles repulsion. Figure 3c shows the spacing between asperities for 20–50 nm Au NPTS at different assembling times. It is clear that the spacing between asperities decreased quickly during the assembling time of 0–6.0 h, after which it decreased slightly. For the 20 nm Au NPTS, the average spacing between asperities is 12.48 nm when the assembling time reaches 24.0 h; however, the average spacing between the 50 nm Au NPs is only about 40.91 nm even if the deposition time reaches to 48.0 h.

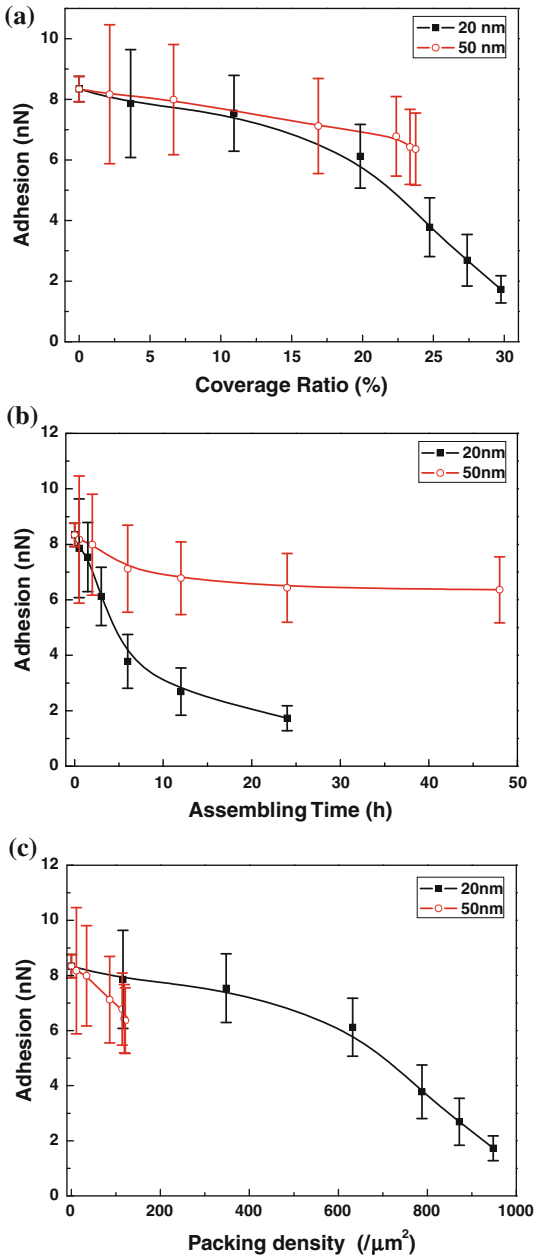

Fig. 4 Adhesive forces for 20–50 nm Au NPTS at different coverage ratio (**a**), assembling time (**b**), and packing density of NPs (**c**)

3.2 Adhesion Studies

Figure 4 shows the adhesive force for the NPTS at different coverage ratio, assembling time, and packing density. For the smooth substrate surface, the coverage ratio of Au NPs was defined as zero. It can be seen that the adhesive forces for 20 nm Au NPTS decreased slightly and then drop rapidly after the coverage ratio beyond 20% (Fig. 4a). For the 50 nm Au NPTS, the adhesive forces decreased slightly with coverage ratio. These results can be explained by the reduction in the real area of contact

between the NPTS surfaces and AFM tip. Based on JKR or DMT models, the adhesive force depends on the interface energy and contact radius [35, 36]. For the case of Si_3N_4 tip-on-smooth substrate surface, the radius of curvature for the contact is determined by the size of AFM tip. The average adhesive force for smooth substrate surface is 8.34 nN. However, for the case of Si_3N_4 tip-on-nanoparticle, the tallest NPs were always selected for the adhesion measurements as the NPs were sparsely distributed on the surface (shown in Figs. 1, 2) [8]. This most likely resulted in single asperity contacts between the AFM tip and the surface, in which case the effective radius of curvature for the contact was determined by both the radii of curvature of nanoparticle in contact and the AFM tip. The reduced real area of contact between the nanoparticle on NPTS and AFM tip results in the effectively reduced adhesion of NPTS. It is found that the average adhesive force for 20 nm Au NPTS assembled for 24.0 h was only about 21% of that for smooth substrate surface. For the 50 nm NPTS, the coverage ratio of NPs is only about 24% even the assembling time reaches to 48.0 h, though, the adhesive force has been reduced by 24% compared to that for the smooth substrate surface.

Figure 4b, c shows the adhesive forces for Au NPTS at different assembling times and different packing densities. For the smooth substrate surface, the assembling time and packing density were also defined as zero. The adhesive force for the NPTS is mainly dependent on the coverage ratio rather than the assembling time or packing density. For instance, with the same assembling time of 24.0 h, the average adhesive forces for NPTS assembled with 20 and 50 nm NPs are 1.73 and 6.43 nN, respectively. Similarly, with the same packing density of about 115 μm^2, the average adhesive forces for NPTS of 0.5 h assembled with 20 nm NPs and 12.0 h assembled with 50 nm NPs are 7.86 and 6.78 nN, respectively. Hence, with the same coverage ratio, the average adhesive forces for different NPTS have minor difference. Besides, it is also observed that the adhesive force has little dependence on the texture height (diameter of nanoparticle) in this study, but closely correlated to the texture coverage ratio on the NPTS surface.

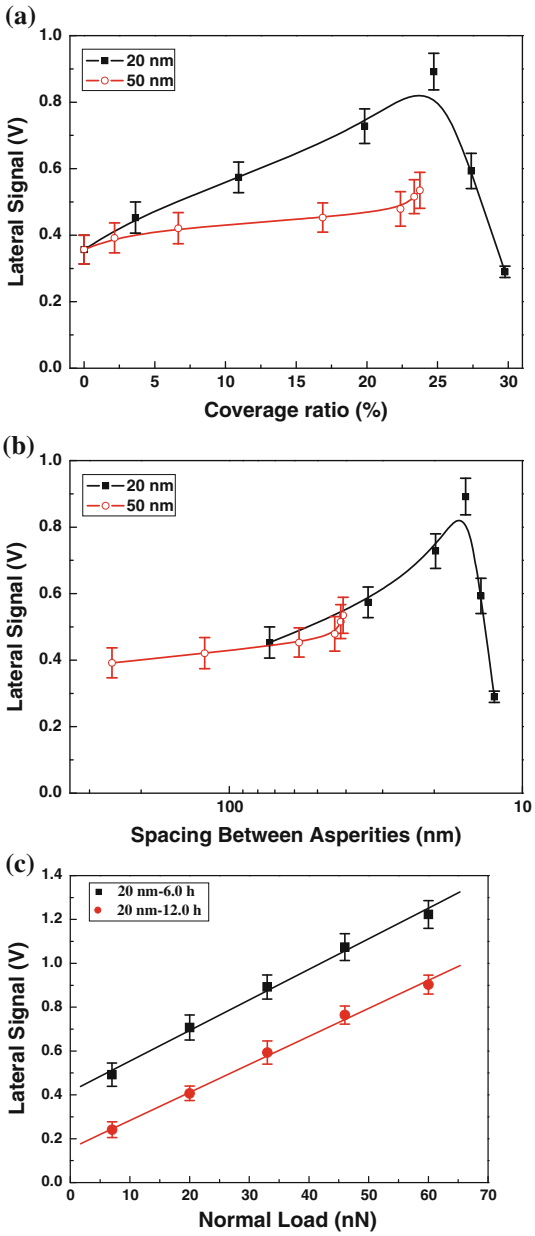

Fig. 5 Frictional forces for Au NPTS at different coverage ratios (**a**), with different spacings between asperities (**b**), and under different normal loads (**c**)

3.3 Friction Studies

Figure 5a, b shows the frictional forces for Au NPTS at different coverage ratios and different spacings between asperities at sliding velocity of 2 μm/s under normal load of 33 nN. As shown in Fig. 5a, the frictional forces for the NPTS assembled with 20 nm Au NPs increased with coverage ratio, and then decreased when coverage ratio is more than 24.74%. However, the frictional forces for NPTS assembled with 50 nm Au NPs continually increased with coverage ratio. Figure 5b shows the effect of spacing between asperities on the frictional forces. It can be seen that the frictional forces for the NPTS assembled with 20 nm Au NPs increased with the decreasing of spacing between asperities, and then decreased when the spacing between asperities is less than 15.62 nm. However, the friction forces for NPTS assembled with 50 nm Au NPs continually increased with the decreasing of spacing between asperities.

In order to better understand the tribological behavior of NPTS, combined with the NPs distribution (Figs. 1, 2), a

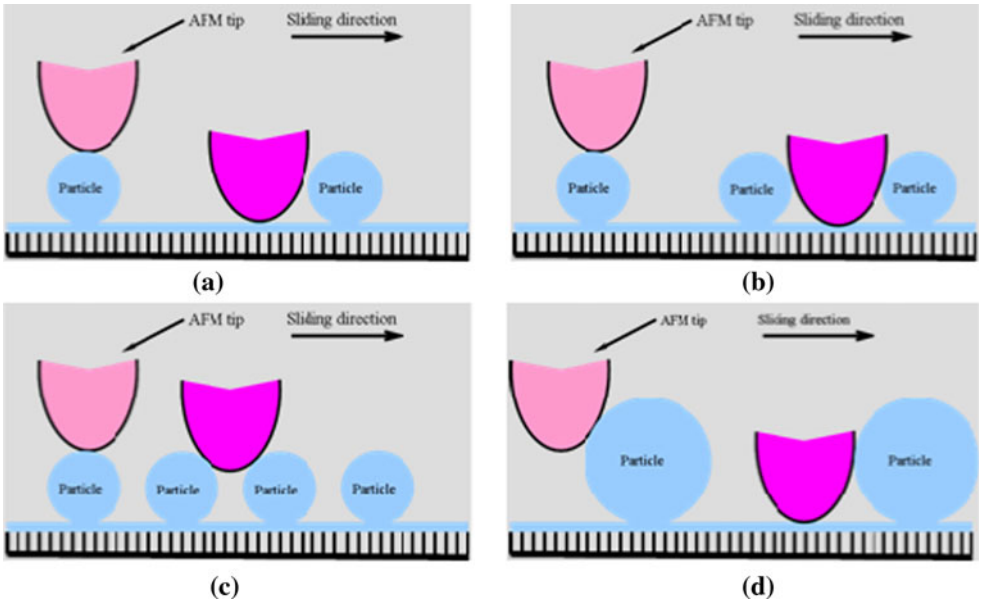

Fig. 6 Schematic diagram of the contact between the AFM tip and NPTS

sketch of the contact established between the AFM tip and the NPTS surfaces is shown in Fig. 6. With the AFM tip sliding over an asperity, the surface slope is positive at the ascending edge, and it is negative at the descending edge. The measured friction force is high at the ascending edge because of the additional torsion of the cantilever beam produced by the collision between the tip and the asperity [37], whereas, at the descending edge, there is no collision effect, and hence no effect on torsion. Moreover, an increase in the amount of friction force experienced by the tip at the ascending edge of an asperity is more than the decrease in the amount of friction force experienced at the descending edge [37]. For the NPTS with a low packing density of the NPs, the spacing between Au NPs is greater than the size of AFM tip. The tip would slide over the NPs on the NPTS surfaces. The theories of continuum contact mechanics were employed to explain the relationship between the AFM tip and 20 nm Au NPTS surfaces, and the friction force is attributed to the friction between tip/smooth substrate surface and tip/NPs as illustrated in Fig. 6a [38]. The 20-nm-radius tip will collide with the asperities but may also come into contact with the flat substrate surface. When the packing density of NPs increased, the quantity of increased frictional force resulting from the collision effect is higher than that of decreased frictional force at the descending edge of an asperity, and thus, the total frictional force increased with the decreasing of spacing between asperities. When the packing density of NPs is high to some extent (i.e., the spacing between asperities is reduced to 15.62 nm), then the tip will "pinch" into the spacing between asperities, and the frictional force between AFM tip and NPTS surface reached the maximum value (Fig. 6b). When the spacing between asperities is further decreased, the AFM tip will slide on the asperities and not come into contact with the substrate surface between the asperities (Fig. 6c). In this case, the AFM tip would be fully in contact with nanoparticle, the effect of collision between the AFM tip and nanoparticle becomes weakened. In addition, the real area of contact between the AFM tip and NPTS was remarkably reduced leading to an obvious descent in the frictional force. As a result, the frictional force can be reduced efficiently when the spacing between the particles is less than the size of tip.

For the NPTS assembled with 50 nm NPs, the frictional force continually increased with the decreasing of spacing between asperities. This is mainly due to the collision effect between the AFM tip and nanoparticle [37]. Because the average spacing between 50 nm NPs is much larger than the size of AFM tip even for the NPTS assembled with 50 nm NPs for 48.0 h, the AFM tip will collide with the asperities and come into contact with the smooth substrate surface between the asperities (Fig. 6d). Because of the collision effect between the tip and asperity, the frictional force increased with the coverage ratio of NPs. Thus, the 50 nm Au NPTS cannot reduce the frictional force in this study, unless the size of tip is larger than the spacing between the NPs.

Figure 5c shows the relationship between the frictional force and the normal load for the NPTS assembled with 20 nm NPs for 6.0–12.0 h at the sliding velocity of 2.0 μm/s, respectively. It can be seen that the frictional force increased linearly with the normal load, and their linear relationship conforms to the modified Amonton's law:

$$F_{\mathrm{L}} = \mu F_{\mathrm{N}} + F_0 \tag{3}$$

where F_{L} is the lateral force (i.e., frictional force), μ is the relative COF, F_{N} is the normal load, and F_0 is the frictional force when the normal load is zero. The increased frictional

force with the normal load can be explained by the enlarged real area of contact. The relative COF for the textured samples assembled with 20 nm NPs for 6.0–12.0 h obtained using a linear fit were found to be 0.0140 and 0.0122, respectively. In other words, the COF for NPTS assembled with 20 nm NPs for 6.0 h is higher than that for 12.0 h. Moreover, the frictional force for NPTS assembled for 6.0 h is higher than that for 12.0 h under each normal load, which is well in agreement with the contact state described above. All in all, the texturing technology is an effective method for controlling the adhesive and frictional properties in nanoscale. In the meantime, the self-assembling of NPs on the silicon surfaces is a convenient way to fabricate controlled nano-textured surfaces. In addition, the contact mechanisms of nano-textured surfaces in nanoscale, and the adhesive and frictional behaviors of nano-textured surfaces measured by tips with different radii of curvature will form the scope of a further investigation in the succeeding research.

4 Conclusions

The NPTS were created by self-assembling Au NPs on the silicon surfaces. The effects of coverage ratio, texture height, and packing density on the nanoscale adhesion and friction of the NPTS were investigated and discussed in detail. The NPTS significantly reduced the adhesion compared to the smooth surface, attributed to the reduced real contact area. The adhesion of NPTS is mainly dependent on the coverage ratio of NPs rather than the texture height and higher coverage ratio resultin in smaller adhesive force. The friction of NPTS is mainly dependent on the spacing between asperities. The lowered frictional force was obtained when the spacing between asperities is less than the size of AFM tip, because of the effectively reduced real area of contact between the AFM tip and the NPTS surface.

Acknowledgments The authors thank the National Natural Science Foundation of China (50972148, 51175490), and ''Hundred Talents Program'' of Chinese Academy of Sciences (KGCX2-YW-804) for funding support extended to this study.

References

1. Menezes, P.L., Kishore, Kailas, S.V.: Studies on friction and transfer layer: role of surface texture. Tribol. Lett. **24**, 265–273 (2006)
2. Lee, H., Bhushan, B.: Role of surface roughness and lubricant film thickness in nanolubrication of sliding components in adaptive optics. J. Colloid Interface Sci. **353**, 574–581 (2011)
3. Burton, Z., Bhushan, B.: Hydrophobicity, adhesion, and friction properties of nanopatterned polymers and scale dependence for micro- and nano-electromechanical systems. Nano Lett. **5**, 1607–1613 (2005)
4. Zhao, W.J., Wang, L.P., Xue, Q.J.: Design and fabrication of nanopillar patterned Au textures for improving nanotribological performance. ACS Appl. Mater. Interface **2**, 788–794 (2010)
5. Nair, R.P., Zou, M.: Surface-nano-texturing by aluminum-induced crystallization of amorphous silicon. Surf. Coat. Technol. **203**, 675–679 (2008)
6. Zou, M., Cai, L., Wang, H., Yang, D., Wyrobek, T.: Adhesion and friction studies of a selectively micro/nano-textured surface produced by UV assisted crystallization of amorphous silicon. Tribol. Lett. **20**, 43–52 (2005)
7. Wang, H., Nair, R.P., Zou, M., Larson, P.R., Pollack, A.L., Hobbs, K.L., et al.: Friction study of a Ni nanodot-patterned surface. Tribol. Lett. **28**, 183–189 (2007)
8. Zou, M., Cai, L., Wang, H.: Adhesion and friction studies of a nano-textured surface produced by spin coating of colloidal silica nanoparticle solution. Tribol. Lett. **21**, 25–30 (2006)
9. Zhang, Y.L., Sundararajan, S.: Adhesion and friction studies of silicon surfaces processed using a microparticle-based method. Tribol. Lett. **23**, 1–5 (2006)
10. Hurst, K.M., Roberts, C.B., Ashurst, W.R.: A gas-expanded liquid nanoparticle deposition technique for reducing the adhesion of silicon microstructures. Nanotechnology **20**, 185303 (2009)
11. Gachot, C., Catrin, R., Lasagni, A., Schmid, U., Mucklich, F.: Comparative study of grain sizes and orientation in microstructured Au, Pt and W thin films designed by laser interference metallurgy. Appl. Surf. Sci. **255**, 5626–5632 (2009)
12. Sugihara, T., Enomoto, T.: Development of a cutting tool with a nano/micro-textured surface-improvement of anti-adhesive effect by considering the texture patterns. Precis. Eng. **33**, 425–429 (2009)
13. Kawasegi, N., Sugimori, H., Morimoto, H., Morita, N., Hori, I.: Development of cutting tools with microscale and nanoscale textures to improve frictional behavior. Precis. Eng. **33**, 248–254 (2009)
14. Nayak, B.K., Gupta, M.C., Kolasinski, K.W.: Formation of nano-textured conical microstructures in titanium metal surface by femtosecond laser irradiation. Appl. Phys. A Mater. **90**, 399–402 (2008)
15. Aditya, L., Srivastava, A., Sahoo, S.K., Das, P., Mukherjee, C., Misra, A., et al.: Growth of textured nanocrystalline cobalt ferrite thin films by pulsed laser deposition. J. Nanosci. Nanotechnol. **8**, 4135–4140 (2008)
16. Sakai, T., Tanaka, Y., Nishizawa, Y., Terakawa, M., Obara, M.: Size parameter effect of dielectric small particle mediated nano-hole patterning on silicon wafer by femtosecond laser. Appl. Phys. A Mater. **99**, 39–46 (2010)
17. Singh, R.A., Yoon, E.S.: Friction of chemically and topographically modified Si (100) surfaces. Wear **263**, 912–919 (2007)
18. Yoon, E.S., Singh, R.A., Kong, H., Kim, B., Kim, D.H., Jeong, H.E., et al.: Tribological properties of bio-mimetic nano-patterned polymeric surfaces on silicon wafer. Tribol. Lett. **21**, 31–37 (2006)
19. Bright, R.M., Musick, M.D., Natan, M.J.: Preparation and characterization of Ag colloid monolayers. Langmuir **14**, 5695–5701 (1998)
20. Tseng, J.Y., Lin, M.H., Chau, L.K.: Preparation of colloidal gold multilayers with 3-(mercaptopropyl)-trimethoxysilane as a linker molecule. Colloid Surf. A **182**, 239–245 (2001)
21. Yuan, B., Xing, L.L., Zhang, Y.D., Lu, Y., Mai, Z.H., Li, M.: Self-assembly of highly oriented lamellar nanoparticle-phospholipid nanocomposites on solid surfaces. J. Am. Chem. Soc. **129**, 11332–11333 (2007)
22. George, C., Ricci, D., Di Zitti, E.: Driving the self assembly of gold nanoparticle structures using highly oriented PTFE templates. Superlattice Microstruct. **44**, 599–607 (2008)

23. Fujiwara, K., Kasaya, H., Ogawa, N.: Gold nanoparticle monolayer formation on a chemically modified glass surface. Anal. Sci. **25**, 241–248 (2009)
24. Lu, K., Hammond, C., Qian, J.M.: Surface patterning nanoparticle-based arrays. J. Mater. Sci. **45**, 582–588 (2010)
25. Marchetto, D., Rota, A., Calabri, L., Gazzadi, G.C., Menozzi, C., Valeri, S.: AFM investigation of tribological properties of nanopatterned silicon surface. Wear **265**, 577–582 (2008)
26. Marchetto, D., Rota, A., Calabri, L., Gazzadi, G.C., Menozzi, C., Valeri, S.: Hydrophobic effect of surface patterning on Si surface. Wear **268**, 488–492 (2010)
27. Doron, A., Katz, E., Willner, I.: Organization of Au colloids as monolayer films onto ITO glass surfaces: application of the metal colloid films as base interfaces to construct redox-active monolayers. Langmuir **11**, 1313–1317 (1995)
28. Chumanov, G., Sokolov, K., Gregory, B.W., Cotton, T.M.: Colloidal metal films as a substrate for surface-enhanced spectroscopy. J. Phys. Chem. **99**, 9466–9471 (1995)
29. Grabar, K.C., Freeman, R.G., Hommer, M.B., Natan, M.J.: Preparation and characterization of Au colloid monolayers. Anal. Chem. **67**, 735–743 (1995)
30. Zhu, T., Zhang, X., Wang, J., Fu, X.Y., Liu, Z.F.: Assembling colloidal Au nanoparticles with functionalized self-assembled monolayers. Thin Solid Films **329**, 595–598 (1998)
31. Huang, X.H., Huang, H.Z., Wu, N.Z., Hu, R.S., Zhu, T., Liu, Z.F.: Investigation of structure and chemical states of self-assembled—Au nanoscale particles by angle-resolved X-ray photoelectron spectroscopy. Surf. Sci. **459**, 183–190 (2000)
32. Delrio, F.W., Dunn, M.L., Boyce, B.L., Corwin, A.D., de Boer, M.P.: The effect of nanoparticles on rough surface adhesion. J. Appl. Phys. **99**, 104304 (2006)
33. Frens, G.: Controlled nucleation for regulation of particle-size in monodisperse gold suspensions. Nat. Phys. Sci. **241**, 20–22 (1973)
34. Keller, D.: Reconstruction of STM and AFM images distorted by finite-size tips. Surf. Sci. **253**, 353–364 (1991)
35. Johnson, K.L., Kendall, K., Roberts, A.D.: Surface energy and contact of elastic solids. Proc. R. Soc. Lond. Soc. A **324**, 301–313 (1971)
36. Derjaguin, B.V., Muller, V.M., Toporov, Y.P.: Effect of contact deformations on adhesion of particles. J. Colloid Interface Sci. **53**, 314–326 (1975)
37. Bhushan, B.: Nanotribology and nanomechanics. Wear **259**, 1507–1531 (2005)
38. Johnson, K.L.: Adhesion and friction between a smooth elastic spherical asperity and a plane surface. Proc. R. Soc. Lond. Soc. A. **453**, 163–179 (1997)